Journal of Catalysis 414 (2022) 179–185

Contents lists available at ScienceDirect

Journal of Catalysis

journal homepage: www.elsevier.com/locate/jcat

Influence of the hydrodynamic size and ζ potential of manganese ferrite nanozymes as peroxidase-mimicking catalysts at pH 4 in different buffers

Carlos Moreno-Castilla [a,*], Ángela Naranjo [b], María Victoria López-Ramón [c,*], Eva Siles [b,*], Jesús J. López-Peñalver [d], José Mariano Ruiz de Almodóvar [e]

[a] Inorganic Chemistry Department, Granada University, 18071 Granada, Spain
[b] Experimental Biology Department, Jaén University, 23071 Jaén, Spain
[c] Inorganic and Organic Chemistry Department, Jaén University, 23071 Jaén, Spain
[d] Experimental Radiology Research Unit, Scientific Instrumentation Center, Granada University, 18071 Granada, Spain
[e] Biomedical Research Center, Granada University, 18071 Granada, Spain

ARTICLE INFO

Article history:
Received 20 July 2022
Revised 8 September 2022
Accepted 9 September 2022
Available online 15 September 2022

Keywords:
Manganese ferrite nanozymes
TMB oxidation
Enzymology methods
Surface science methods
Heterogeneous catalysis
Surface coating
Hydrodynamic size
ζ potential
Fenton process

ABSTRACT

Peroxidase-mimicking activity of manganese ferrite nanoparticles was studied, based on the oxidation of TMB (3,3′,5,5′-tetramethylbenzidine) by H_2O_2 at pH 4 using acetate and citrate buffers. The aim of this study was to examine this reaction not only by enzymology (Michaelis-Menten kinetics model) but also by surface science methods of heterogeneous catalysis. Nanoparticles were characterized by different techniques to determine their phase composition, surface area, surface composition, surface charge, pH at the point of zero charge, magnetization, mean size, and morphology. Results show that the nanozymes are coated with buffer anions that form a shell around them. In addition, the hydrodynamic size and ζ potential of the nanoparticles under reaction conditions play an important role in the proposed Fenton-type oxidation mechanism. A greater amount of Mn ions than Fe ions leaches from the nanozymes during TMB oxidation, likely because Fe is better protected than Mn by the buffer coating the outer surface of the nanoparticles. This shortcoming must be addressed when applying these nanomaterials.

1. Introduction

Enzymes are biological catalysts that participate in most reactions taking place in living organisms [1]. Peroxidase enzymes belong to a large family that generally uses H_2O_2 to oxidize the substrate and are important free radical detoxifying agents for defense against invading pathogens [2], for the oxidation of different organic substrates in wastewater treatments, and for utilization as detection tools [3]. The discovery that magnetite nanoparticles behave similarly to horse radish peroxidase enzyme, yielding the same oxidation product [3], led to the preparation of other inorganic nanoparticles that mimic the catalytic activity of different biological enzymes, including oxidase, catalase, haloperoxidase, glutathione peroxidase, uricase, methane monooxygenase, hydrolase, and superoxide dismutase (SOD) [4,5]. These inorganic nanoparticle catalysts are called nanozymes, although they likely have distinct reaction mechanisms [6–8]. It was recently questioned [9] whether some magnetic nanomaterials with intrinsic peroxidase-like activity in the presence of H_2O_2 are true nanozymes, mainly due to their oxidation mechanism. This can follow: (i) the specific reaction of peroxidase enzymes, which is a two-electron oxidation mechanism; or (ii) a Fenton type mechanism in which $HO^{\bullet}$ radicals that oxidize the substrate are generated on the surface of the nanomaterial.

Advantages of nanozymes over enzymes include their avoidance of some of the drawbacks of the latter, such as their low stability, difficult storage, high synthesis cost, and sophisticated purification techniques [5,8], explaining the major interest in nanozymes over recent years [9]. Nanozymes are, therefore, related to enzymology and heterogeneous catalysis. In normal practice, nanozyme activity has been widely described by the Michaelis-Menten (M–M) kinetics model, which implies an enzymology approach [8]. However, given that nanozymes are heterogeneous catalysts, the application of surface science concepts and

* Corresponding authors.
E-mail addresses: cmoreno@ugr.es (C. Moreno-Castilla), mvlro@ujaen.es (M. Victoria López-Ramón), esiles@ujaen.es (E. Siles).

https://doi.org/10.1016/j.jcat.2022.09.010
0021-9517/

methods can provide new insights into the reaction mechanisms of these nanomaterials [4,8–10].

The objective of this investigation was therefore to study manganese ferrite nanoparticles as nanozymes that mimic peroxidase catalysts to oxidize TMB in a heterogeneous catalysis approach, although the M–M kinetics model is also applied. Two manganese ferrite nanomaterials were used for this purpose: as-prepared (MSN), and calcined at 350 °C (MSN350). TMB oxidation is conducted at pH 4, an essential requirement [2], using acetate and citrate buffers.

Surface science methods were used to determine the size, morphology, and surface charge of the nanomaterials under reaction conditions, studying the hydrodynamic size by dynamic light scattering (DLS), the size and morphology by transmission electron and atomic force microscopies (TEM and AFM, respectively), and the surface charge by ζ potential. The TMB molecular size and surface charge at pH 4 was also investigated to determine the nature of the electrostatic interactions between nanoparticles and substrate. Data were also obtained on M–M kinetic parameters, turnover frequency (TOF), and activation energy of the corresponding reactions and were related to the hydrodynamic size of the nanomaterials in solution and their surface composition. Results obtained underlie the proposal of a reaction mechanism for the nanoparticles used.

2. Materials and methods

2.1. Materials

Iron (III) chloride hexahydrate and manganese (II) chloride tetrahydrate, TMB, acetic acid, tri-sodium citrate, ethylene glycol, ethylenediamine, sodium acetate, and dimethyl sulfoxide (DMSO) were analytical grade reagents supplied by Sigma Aldrich. Ethanol absolute (100%) was provided by VWR Chemical and H_2O_2 (30% wt %) by Panreac Applichem. All reagents were used as-received with no further purification.

2.2. Preparation of $MnFe_2O_4$ solid nanospheres

MSN was prepared following a previously reported solvothermal method [11], and MSN350 was obtained after calcining MSN at 350 °C in an air-oven for 4 h, as described elsewhere [12]. Details of the synthesis are given in Text S1 of Supplementary material.

2.3. Characterization methods

The crystallographic structure of the two samples was determined by XRD, and their morphology was characterized by TEM. The specific surface area, S_{BET}, was obtained by applying the BET equation to the N_2 adsorption isotherms at −196 °C. The pH_{PZC} was obtained by potentiometric titrations. Data were also obtained on the magnetization of the nanozymes against the applied external magnetic field applied. XPS studies were also conducted. Mean nanozyme size was measured by TEM, DLS, and AFM, and the ζ potential of nanozymes was determined at pH 4 in each buffer. The characterization techniques employed are described in detail in Text S1 of Supplementary material.

2.4. Assays of the peroxidase-mimicking activity of nanozymes

Determination of the peroxidase-mimicking activity of MSN and MSN350 was based on the oxidation of TMB by H_2O_2 and application of the M–M kinetics model. Different concentrations of nanozymes were assayed with a fixed H_2O_2 concentration to obtain the TOF of their peroxidase-mimicking activity. Finally, the activation energy was obtained between 25 and 35 °C. The activity assays are described in detail in Text S1 of Supplementary material.

3. Results and discussion

3.1. Characteristics of nanozymes and the TMB substrate

Fig. 1 depicts the morphology of MSN and MSN350 catalysts from TEM, showing them to be composed of nanospherical particles formed by the heterojunction of smaller spherical building blocks. Tables 1 and 2 display most of the surface characteristics reported and discussed elsewhere [12]. Briefly, the calcination treatment of MSN at 350 °C to obtain MSN350 changes its surface characteristics. For instance, X-ray diffraction (XRD) patterns (Fig. S1 of Supplementary material) reveal that cubic spinel jacobsite is oxidized to non-stoichiometric maghemite ($MnFe_2O_{4+\delta}$) and there are reductions in crystal size, BET surface area, pH at the point zero charge (pH_{PZC}), and saturation magnetization (M_S). However, there is no change in remnant magnetization (M_R) or coercivity (H_C). The high M_S value of the two ferrites permits their ready separation from the solution using an external magnet.

X-ray photoelectron spectroscopy (XPS) results are displayed in Table 2, and the corresponding spectra are depicted in Figs. S2 and S3. Both ferrites show $2p_{3/2}$ peaks at around 710 and 711 eV, attributed to Fe(III) in B (octahedral) and A (tetrahedral) sites, respectively. Hence, they have a partially inverted spinel structure. In

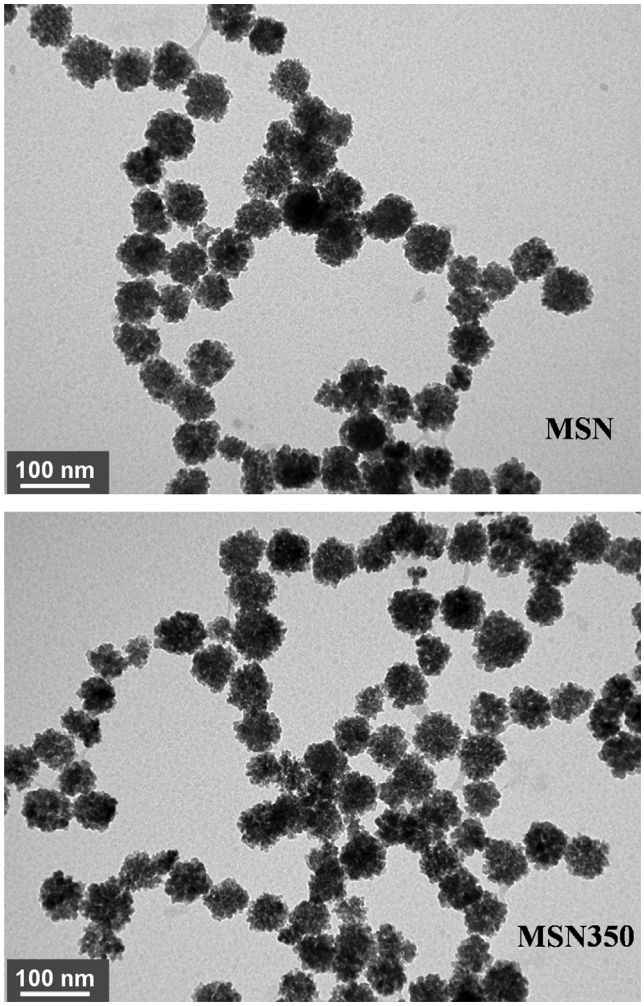

Fig. 1. TEM micrographs of MSN and MSN350.

Table 1
Results from XRD patterns, BET surface area, pH_{PZC} and magnetic behavior of nanozymes.

Nanozyme	Crystal phase	Crystal size nm	S_{BET} $m^2\ g^{-1}$	pH_{PZC}	M_S emu g^{-1}	M_R emu g^{-1}	H_C kOe
MSN	Jacobsite	10.2	138	8.0	54.3	2.4	0.03
MSN350	Maghemite	8.0	104	7.0	43.7	2.5	0.04

Table 2
Binding energy (eV) of the main XPS peaks of the nanozymes with percentage (in parentheses), Fe, Mn and O atomic percentages and Mn/Fe atomic ratio.

Nanozyme	Fe $2p_{3/2}$ eV	Fe_{at} %	Mn $2p_{3/2}$ eV	Mn_{at} %	Mn/Fe	O $_{1s}$ eV	O_{at} %
MSN	710.1 (32) 711.4 (68)	19.2	640.6 (65) 641.7 (35)	9.5	0.49	529.7 (71) 531.4 (29)	71.3
MSN350	709.9 (30) 711.2 (70)	15.6	641.1 (66) 642.4 (34)	12.2	0.78	529.6 (73) 531.2 (27)	72.2

regard to Mn, MSN shows the presence of Mn(II) and Mn(III) with $2p_{3/2}$ peaks at 640.6 and 641.7 eV, respectively, whereas MSN350 has peaks at 641.1 and 642.4 eV, attributed to Mn(III) and Mn (IV), respectively. The Mn/Fe atomic ratio is very close to 0.5, the theoretical value of the manganese ferrite spinel. However, this ratio is increased in MSN350 due to Mn segregation to the ferrite surface. Finally, two O_{1s} peaks at around 529.6 and 531.2 eV are attributed to surface lattice oxygen and surface –OH groups, respectively [12].

Mean sizes of ferrite nanoparticles, from various techniques, are displayed in Table 3. Mean hydrodynamic size by DLS is higher than the mean size by TEM in water due to the hydrophilic character of the nanozyme surface and its consequent hydration. Suspension of the nanozymes in acetate or citrate buffers produces a major increase in their mean hydrodynamic size, indicating a greater attraction to the nanozyme surface for the buffers than for water. This is because the surfaces of both ferrites are positively charged at the working pH (4.0) used for the peroxidase reaction due to their pH_{PZC} (Table 1), and they would therefore strongly attract acetate and citrate anions in the suspension. Mean nanozyme sizes are the same by AFM and TEM in water, and the mean size is markedly lower by AFM than by DLS in both buffers. This is attributable to evaporation of the solvent before the AFM measurement, leading to desorption of some of the water, acetate, or citrate adsorbed on the nanozymes. Fig. 2 depicts some AFM micrographs of the two ferrites in different media, showing that nanozymes are coated with buffer anions that form a shell around them. More information about this coating is given in Figs. S4 and S5.

The coating of nanozyme surfaces by water or buffer anions affects not only their size but also their ζ potential (Table 4). In this way, MSN350 shows a more negative ζ potential in water and acetate buffer in comparison to MSN, attributable to the presence of Mn(IV). Hence, Mn^{4+}— OH complexes are readily formed in aqueous solution due to the dissociative adsorption of water molecules [13], attracting OH^- ions from the water. For their part, acetate ions are also attracted by Mn(IV) to the MSN350 surface due to their negative charge. However, the two nanozymes have the same ζ potential in citrate buffer, which coats their surface and forms a coordination complex with the surface metal ions due to the citric-citrate complexation capacity [14,15]. In addition, all nanozyme particles coated by buffer anions are negatively charged in the studied media, and repulsive interactions among them would prevent their agglomeration [16].

To our best knowledge, this is the first report that nanozymes are coated by the anions of buffers used to control the suspension pH for the reaction. Unlike in the case of biological enzymes, this phenomenon is widespread in these types of material due to the presence of metal ions in different oxidation states on their surfaces. Hence, the surface coating of nanozymes is one of the most important differences between the two types of catalyst, inorganic nanozymes and biological enzymes.

Fig. 3 depicts the molecular structure of TMB. It has a molecular volume of 0.37 nm^3 and a Van der Waals surface area of 3.98 nm^2 [17]. The pK_a and dipole moment of TMB are 4.17 and 0.42 D, respectively [18]. With two amino groups, the non-oxidized TMB is partially positively charged at pH 4 [19].

3.2. Manganese ferrite nanozymes as peroxidase catalysts.

Nanozymes share many features with enzymes but are heterogeneous inorganic catalysts rather than biological catalysts. Nevertheless, nanozyme activity has usually been described with the M–M kinetics model, involving the application of enzymology methods [2,4,5,8,20,21]. Fig. 4A depicts the activity of MSN and MSN350 nanozymes at 25 °C as a function of TMB concentration in acetate and citrate buffers. The results of applying the M–M kinetics model to these curves are compiled in Table 5. K_m is the M–M catalytic constant, V_{max} is the maximum reaction rate, and k_{cat} is the V_{max} per surface area unit of the nanozyme. This is an enzymology term, whereas the TOF is more frequently used in heterogeneous catalysis [8]. The surface area was considered in the present study because enzymes typically have one active site, whereas nanozymes, as in the case of heterogeneous catalysts, have more than one active center (metal ions) on their surface.

As shown in Table 5, MSN350 has the highest k_{cat} value in acetate buffer and MSN the highest value in citrate buffer. This is related to the mean hydrodynamic size of the nanozymes (Table 3),

Table 3
Mean nanozyme size (nm) by various techniques.

Nanozyme	TEM	DLS			AFM		
		Water	Acetate buffer	Citrate buffer	Water	Acetate buffer	Citrate buffer
MSN	75 ± 5	127 ± 2	2971 ± 77	1400 ± 70	74 ± 1	158 ± 4	194 ± 5
MSN350	75 ± 5	130 ± 2	1802 ± 69	1704 ± 86	77 ± 1	248 ± 7	337 ± 13

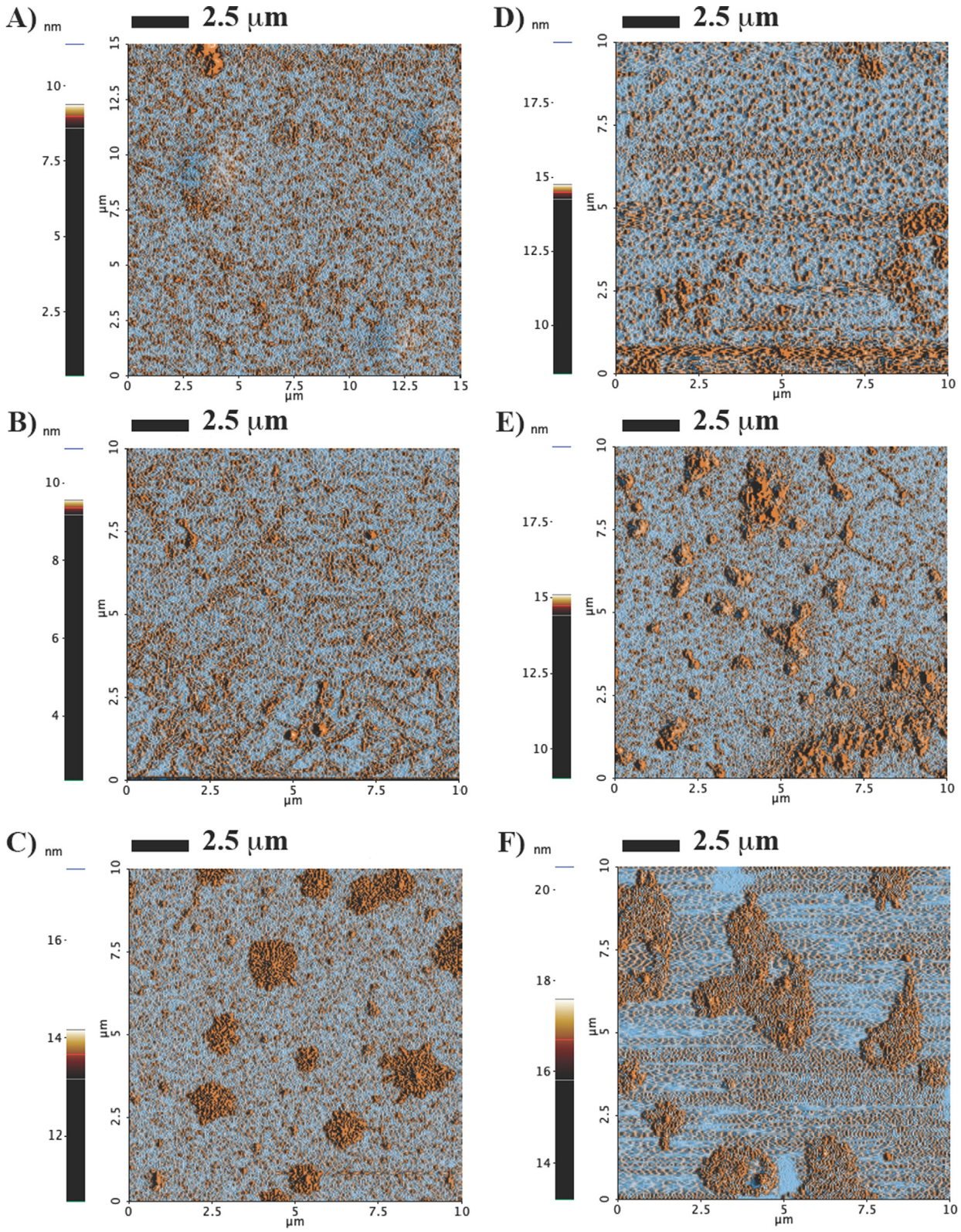

Fig. 2. AFM micrographs of (A) MSN-H_2O; (B) MSN-Acetate; (C) MSN-Citrate; (D) MSN350-H_2O; (E) MSN350-Acetate; (F) MSN350-Citrate.

Table 4
ζ potentials (mV) of nanozymes in different media.

Nanozyme	Water	Acetate buffer	Citrate buffer
MSN	−20.3 ± 0.3	−8.7 ± 0.5	−19.7 ± 1.1
MSN350	−33.9 ± 1.0	−13.4 ± 0.6	−19.7 ± 1.9

given that the nanozyme with lowest mean hydrodynamic size in each buffer has the highest k_{cat} value. Table 5 does not report the k_{cat}/K_m ratio, which should only be used to compare reaction rates of different substrates catalyzed by the same enzyme and not to compare the catalytic efficacy of different enzymes [16,22].

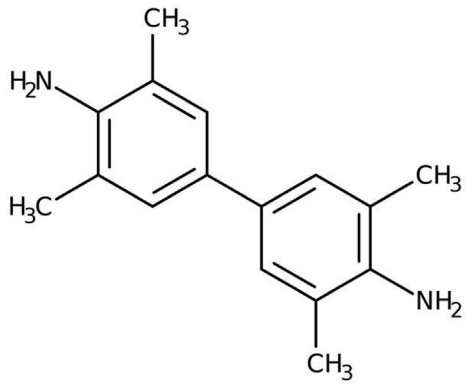

Fig. 3. TMB molecular structure.

TOF values at 25 °C and activation energies between 25 and 35 °C were calculated from Fig. 4B and 4C, respectively, and the results are displayed in Table 6. They indicate that the nanozyme with the lowest mean hydrodynamic size in each buffer has the highest TOF value and the lowest activation energy. TOF results evidence a similar trend to that observed for k_{cat} results, and Fig. 4D shows the linear relationship (0.9705 correlation coefficient) between k_{cat} and TOF values. Finally, the results indicate that the DLS-estimated mean hydrodynamic size of the nanozyme plays a key role in its activity, being of major importance in the first steps of the TMB oxidation mechanism, as described below.

The proposed Fenton-type TMB oxidation mechanism is depicted in Scheme 1. Under reaction conditions, pH 4, the TMB is partially positively charged and would be electrostatically attracted by the negatively charged coating of the nanozymes. According to the ζ potentials (Table 4), attractive interactions would be higher for MSN350 in acetate buffer but would not differ between these nanozymes in citrate buffer. Consequently, TMB cannot pass through the buffer coating to reach the nanozyme surface. In contrast, H_2O_2 can reach the nanozyme surface more readily, which depends on the mean hydrodynamic size, because of its much lower molecular volume (0.004 nm^3) and Van der Waals surface area (0.49 nm^2) in comparison to TMB (0.37 nm^3 and 3.98 nm^2, respectively). It would decompose on the surface into HO· radicals according to Eqs. (1)–(6) [23,24], which would oxidize the TMB attached to the outer coating of the nanozymes.

$$Fe^{2+} + H_2O_2 \rightarrow Fe^{3+} + OH^- + HO^\bullet \quad (1)$$

$$Fe^{3+} + H_2O_2 \rightarrow Fe^{2+} + H^+ + HO_2^\bullet \quad (2)$$

$$Mn^{2+} + H_2O_2 \rightarrow Mn^{3+} + OH^- + HO^\bullet \quad (3)$$

$$Mn^{3+} + H_2O_2 \rightarrow Mn^{2+} + H^+ + HO_2^\bullet \quad (4)$$

$$Mn^{4+} + H_2O_2 \rightarrow Mn^{3+} + H^+ + HO_2^\bullet \quad (5)$$

$$Mn^{3+} + H_2O_2 \rightarrow Mn^{4+} + OH^- + HO^\bullet \quad (6)$$

On the other hand, Mn and Fe ions leach from the nanozymes during TMB oxidation (Table 7). There is practically no difference in the amounts of ions leached between reaction temperatures of 25 and 35 °C. The amount of Mn leached from MSN is similar in each buffer, while a larger amount leaches from MSN350 due to the surface segregation of Mn detected by XPS, with little difference between buffers. In comparison to Mn, a much smaller amount of Fe is leached from MSN and MSN350 in acetate and

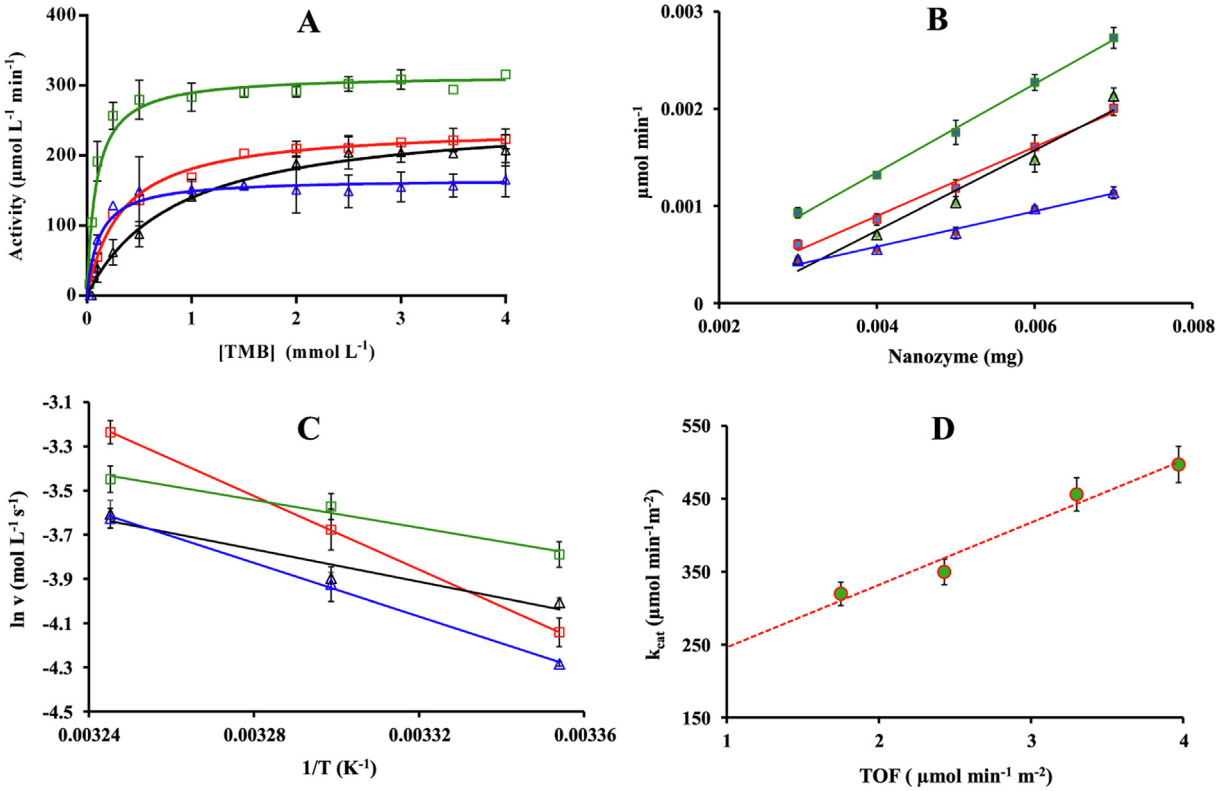

Fig. 4. (A) Activity of nanozymes against TMB concentration at 25 °C; $[H_2O_2]$ = 10 mM and [Nanozyme] = 2.17×10^{-5} M. (B) Relationship between nanozyme activity at 25 °C and their mass. [TMB] = 4 mM; $[H_2O_2]$ = 10 mM. (C) Arrhenius plots at temperatures between 25 and 35 °C; [TMB] = 4 mM; $[H_2O_2]$ = 10 mM and [Nanozyme] = 2.17×10^{-5} M. (D) Relationship between k_{cat} and TOF.

Table 5
Michaelis-Menten kinetic parameters of MSN nanozymes in different buffers (pH 4). [Nanozyme] = 2.17x10^{-5} M; [H_2O_2] = 10 mM; [TMB] up to 4 mM.

Nanozyme/Buffer	K_m mmol L^{-1}	V_{max} µmol L^{-1} min^{-1}	k_{cat} µmol min^{-1} m^{-2}	R^2
MSN/Acet.	0.335	241.5	349.5	0.976
MSN350/Acet.	0.855	259.0	497.1	0.960
MSN/Citr.	0.089	315.1	456.0	0.934
MSN350/Citr.	0.119	166.6	319.8	0.848

Table 6
TOF at 25 °C and activation energies between 25 and 35 °C of the nanozymes in the TMB oxidation reaction.

Nanozyme/Buffer	TOF µmol min^{-1} m^{-2}	Activation energy kJ mol^{-1}
MSN/Acet.	2.43 ± 0.14	69.2 ± 4.8
MSN350/Acet.	3.97 ± 0.10	30.5 ± 1.1
MSN/Citr.	3.30 ± 0.19	26.1 ± 1.5
MSN350/Citr.	1.75 ± 0.08	50.4 ± 2.2

citrate buffers under the same conditions, although the amount of Fe leached in citrate buffer from both nanozymes was slightly higher than that leached in acetate buffer.

The finding that much more Mn than Fe is leached by MSN and MSN350 in both buffers contrasts with observations for the same catalysts in the oxidation of *para*-nitrophenol with potassium peroxymonosulfate at 40 °C in unbuffered solution, with initial and final pHs of 5.8 and 2.6, respectively [12]. One explanation is that Fe is better protected than Mn by the buffer that coats the outer surface of the nanoparticles, likely due to the formation of more stable coordination complexes with Fe than with Mn ions on their surface.

Leaching of metal ions is typically observed from heterogeneous inorganic catalysts in aqueous solutions at certain pH values but not from enzymatic catalysts. According to the EPA, the maximum permitted Mn concentration in water is 0.05 mg L^{-1} [25], much lower than the concentrations observed with these nanomaterials. The leaching of metal ions from the surface of nanomaterials is a major problem that must be addressed when they are used as an enzymatic-mimicking catalyst, given their negative impact not only on the integrity of the heterogeneous catalyst but also on the environment.

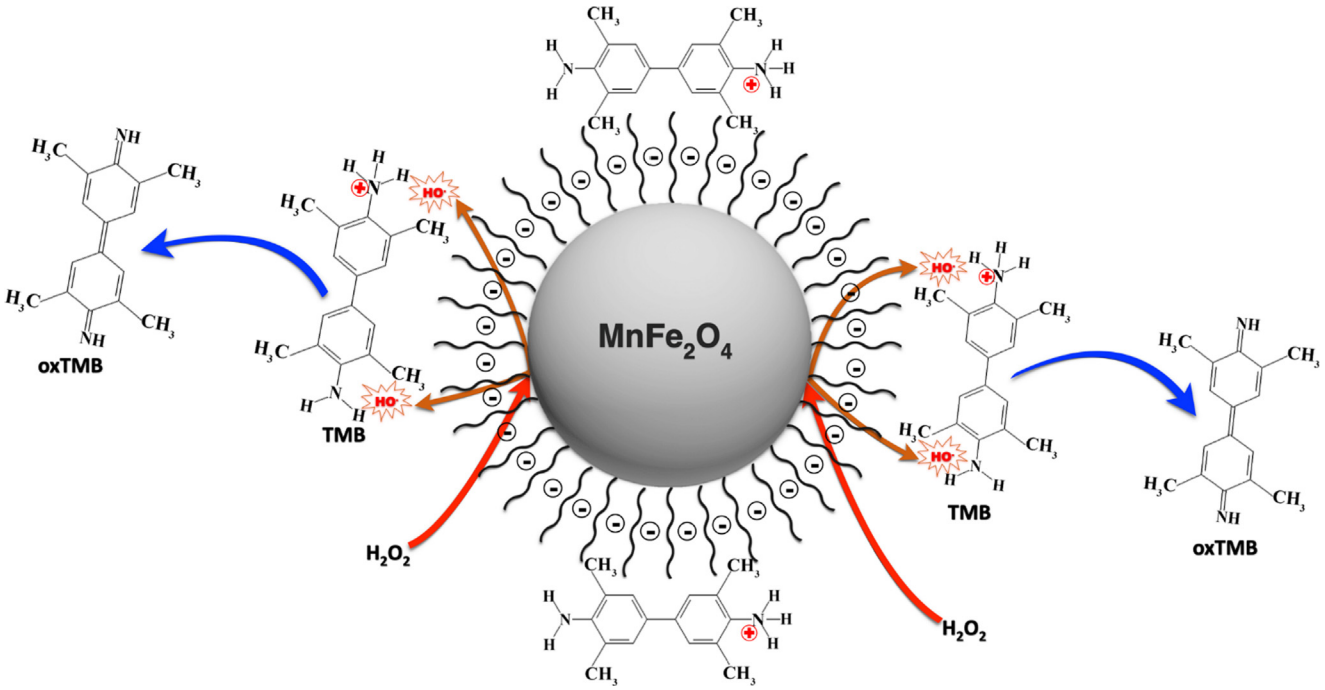

Scheme 1. TMB oxidation mechanism proposed.

Table 7
Metal ions leached after 5 min of reaction. [Nanozyme] = 2.17x10^{-5} M; [H_2O_2] = 10 mM; [TMB] = 4 mM.

Nanozyme	T (°C)	Acetate buffer		Citrate buffer	
		$Mn_{leached}$ mg L^{-1}	$Fe_{leached}$ mg L^{-1}	$Mn_{leached}$ mg L^{-1}	$Fe_{leached}$ mg L^{-1}
MSN	25	0.32	0.03	0.27	0.08
	30	0.27	0.02	0.29	0.09
	35	0.35	0.03	0.32	0.11
MSN350	25	0.49	0.04	0.43	0.11
	30	0.46	0.04	0.47	0.13
	35	0.48	0.05	0.48	0.13

4. Conclusions

Nanozymes are coated with the anions of buffers employed to control the suspension pH at which reactions take place, because their surfaces contain metal ions in different oxidation states. This phenomenon is not observed with biological enzymes. Hence, this surface coating is one of the main differences between inorganic nanozymes and biological enzymes. The nanozyme with the lowest mean hydrodynamic size in each buffer has the highest k_{cat} and TOF values and the lowest activation energy. A Fenton type mechanism is proposed to explain the TMB oxidation at pH 4 with acetate and citrate buffers. Finally, Mn and Fe ions leach from the surface of the nanozymes during TMB oxidation. This leaching is typically observed when heterogeneous inorganic catalysts are used in solutions and must be addressed when using nanozymes, because it can negatively affect the integrity of the heterogeneous catalyst and the environment.

Finally, future research is warranted on buffers that minimize the coating of the nanozyme particles and avoid the leaching of metal ions from their surfaces. Once this is achieved, it will be of major interest, given the deleterious role of oxidative stress in numerous pathologies such as stroke, to evaluate the potential therapeutic effect of these nanozymes in *in vitro* and *in vivo* models of this and other diseases.

CRediT authorship contribution statement

Carlos Moreno-Castilla: Conceptualization, Supervision, Writing – review & editing. **Ángela Naranjo:** Investigation, Formal analysis. **María Victoria López-Ramón:** Investigation, Formal analysis, Funding acquisition. **Eva Siles:** Investigation, Formal analysis. **Jesús J. López-Peñalver:** Investigation, Formal analysis. **José Mariano Ruiz de Almodóvar:** Methodology, Formal analysis.

Declaration of Competing Interest

The authors declare that they have no known competing financial interests or personal relationships that could have appeared to influence the work reported in this paper.

Acknowledgements

M.V.L-R and C.M-C acknowledge financial support from the FEDER 2014-2020 Operative Program, and Junta de Andalucía, Spain. (Projects FEDER-UJA-1380629). C.M-C thanks Dr Mila Gómez for her support in the manuscript preparation. Funding for open access charge; Universidad de Granada/CBUA.

Appendix A. Supplementary material

Supplementary data to this article can be found online at https://doi.org/10.1016/j.jcat.2022.09.010.

References

[1] Enzymes: A Very Short Introduction, Paul Engel 2020, first ed., Oxford University Press.
[2] S. Singh, Nanomaterials exhibiting enzyme-like properties (nanozymes): current advances and future perspectives, Front. Chem. 7 (2019) 46, https://doi.org/10.3389/fchem.2019.00046.
[3] L. Gao, J. Zhuang, L. Nie, J. Zhang, Y. Zhang, N. Gu, T. Wang, J. Feng, D. Yang, S. Perrett, X. Yan, Intrinsic peroxidase-like activity of ferromagnetic nanoparticles, Nat. Nanotechnol. 2 (2007) 577–583, https://doi.org/10.1038/nnano.2007.260.
[4] M. Liang, X. Yan, Nanozymes: from new concepts, mechanisms, and standards to applications, Acc. Chem. Res. 52 (8) (2019) 2190–2200, https://doi.org/10.1021/acs.accounts.9b00140.
[5] E. Hermosilla, A.B. Seabra, I.M. Lourenço, F.F. Ferreira, G. Tortella, O. Rubilar, Highly sensitive oxidation of MBTH/DMAB by $MnFe_2O_4$ nanoparticles as a promising method for nanozyme-based sensor development, Colloids Surf. A: Physicochem. Eng. Asp. 621 (2021) 126585, https://doi.org/10.1016/j.colsurfa.2021.126585.
[6] H. Wei, L. Gao, K. Fan, J. Liu, J. He, X. Qu, S. Dong, E. Wang, X. Yan, Nanozymes: a clear definition with fuzzy edges, Nano Today 40 (2021) 101269, https://doi.org/10.1016/j.nantod.2021.101269.
[7] B. Yuan, H.-L. Chou, Y.-K. Peng, Disclosing the origin of transition metal oxides as peroxidase (and catalase) mimetics, ACS Appl. Mater. Interfaces 14 (20) (2022) 22728–22736, https://doi.org/10.1021/acsami.1c13429.
[8] M. Zandieh, J. Liu, Surface science of nanozymes and defining a nanozyme unit, Langmuir 38 (12) (2022) 3617–3622, https://doi.org/10.1021/acs.langmuir.2c00070.
[9] A. Robert, B. Meunier, How to define a nanozyme, ACS Nano 16 (5) (2022) 6956–6959, https://doi.org/10.1021/acsnano.2c02966.
[10] P. Wang, T. Wang, J. Hong, X. Yan, M. Liang, Nanozymes: a new disease imaging strategy, Front. Bioeng. Biotechnol. 8 (2020) 15, https://doi.org/10.3389/fbioe.2020.00015.
[11] M. Li, Q. Gao, T. Wang, Y.-S. Gong, B. Han, K.-S. Xia, C.-G. Zhou, Solvothermal synthesis of $MnxFe_{3\_}xO4$ nanoparticles with interesting physicochemical characteristics and good catalytic degradation activity, Mater. Design 97 (2016) 341–348, https://doi.org/10.1016/j.matdes.2016.02.103.
[12] L. Mateus, C. Moreno-Castilla, M.V. López-Ramón, F.B. Cortés, M.A. Álvarez, O.E. Medina, C.A. Franco, A. Yebra-Rodríguez, Physicochemical characteristics of calcined $MnFe_2O_4$ solid nanospheres and their catalytic activity to oxidize *para*-nitrophenol with peroxymonosulfate and *n*-C_7 asphaltenes with air, J. Environ. Manage. 281 (2021) 111871, https://doi.org/10.1016/j.jenvman.2020.111871.
[13] J. Deng, S. Feng, X. Ma, C. Tan, H. Wang, S. Zhou, T. Zhang, J. Li, Heterogeneous degradation of orange II with peroxymonosulfate activated by ordered mesoporous $MnFe_2O_4$, Sep. Purif. Technol. 167 (2016) 181–189, https://doi.org/10.1016/j.seppur.2016.04.035.
[14] I. Gautier-Luneau, C. Merle, D. Phanon, C. Lebrun, F. Biaso, G. Serratrice, J.-L. Pierre, New trends in the chemistry of iron(III) citrate complexes: correlations between X-ray structures and solution species probed by electrospray mass spectrometry and kinetics of iron uptake from citrate by iron chelators, Chem. Eur. J. 11 (2005) 2207–2219, https://doi.org/10.1002/chem.200401087.
[15] D. Wyrzykowski, L. Chmurzynski, Thermodynamics of citrate complexation with Mn^{2+}, Co^{2+}, Ni^{2+} and Zn^{2+} ions, J. Therm. Anal. Calorim. 102 (2010) 61–64, https://doi.org/10.1007/s10973-009-0523-4.
[16] H. Han, W. Yin, D. Wang, Z. Zhu, B. Yang, J. Yao, New insights into the dispersion mechanism of citric acid for enhancing the flotation separation of fine siderite from hematite and quartz, Colloids Surf. A: Physicochem. Eng. Asp. 641 (2022) 128459, https://doi.org/10.1016/j.colsurfa.2022.128459.
[17] ACD/Labs Software, Advanced Chemistry Development Inc. <http://www.chemspider.com>.
[18] K.-T. Chung, S.-C. Chen, T.Y. Wong, Y.-S. Li, C.-I. Wei, M.W. Chou, Mutagenicity studies of benzidine and its analogs: structure-activity relationships, Toxicol. Sci. 56 (2000) 351–356, https://doi.org/10.1093/toxsci/56.2.351.
[19] B. Liu, J. Liu, Accelerating peroxidase mimicking nanozymes using DNA, Nanoscale 7 (33) (2015) 13831–13835, https://doi.org/10.1039/C5NR04176G.
[20] C.A.S. Ballesteros, L.A. Mercante, A.D. Alvarenga, M.H.M. Facure, R. Schneider, D.S. Correa, Recent trends in nanozymes design: from materials and structures to environmental applications, Mater. Chem. Front. 5 (20) (2021) 7419–7451, https://doi.org/10.1039/D1QM00947H.
[21] L.J. Peng, H.Y. Zhou, C.Y. Zhang, F.Q. Yang, Study on the peroxidase-like activity of cobalt phosphate and its application in colorimetric detection of hydrogen peroxide, Colloids Surf. A: Physicochem. Eng. Asp. 647 (2022) 129031, https://doi.org/10.1016/j.colsurfa.2022.129031.
[22] R. Eisenthal, M.J. Danson, D.W. Hough, Catalytic efficiency and k_{cat}/K_M: a useful comparator?, Trends Biotechnol 25 (6) (2007) 247–249, https://doi.org/10.1016/j.tibtech.2007.03.010.
[23] M.V. López-Ramón, M.A. Álvarez, C. Moreno-Castilla, M.A. Fontecha-Cámara, A. Yebra-Rodríguez, E. Bailón-García, Effect of calcination temperature of a copper ferrite synthesized by a sol-gel method on its structural characteristics and performance as Fenton catalyst to remove gallic acid from water, J. Colloid Interface Sci. 511 (2018) 193–202, https://doi.org/10.1016/j.jcis.2017.09.117.
[24] A. Shokri, M.S. Fard, A critical review in Fenton-like approach for the removal of pollutants in the aqueous environment, Environ. Challeng. 7 (2022) 100534, https://doi.org/10.1016/j.envc.2022.100534.
[25] J.M. Cerrato, M.F. Hochella Jr., W.R. Knocke, A.M. Dietrich, T.F. Cromer, Use of XPS to identify the oxidation state of Mn in solid surfaces of filtration media oxide samples from drinking water treatment plants, Environ. Sci. Technol. 44 (2010) 5881–5886, https://doi.org/10.1021/es100547q.